Neutron powder diffraction study of the two-dimensional triangular lattice antiferromagnet $CuCrO_2$

1990 J. Phys.: Condens. Matter 2 4485

(http://iopscience.iop.org/0953-8984/2/19/014)

J. Phys.: Condens. Matter **2** (1990) 4485–4493. Printed in the UK

Neutron powder diffraction study of the two-dimensional triangular lattice antiferromagnet $CuCrO_2$

H Kadowaki†, H Kikuchi‡§ and Y Ajiro‡
† Institute for Solid State Physics, The University of Tokyo, Roppongi, Minato-ku, Tokyo 106, Japan
‡ Department of Chemistry, Faculty of Science, Kyoto University, Kitashirakawa, Sakyo-ku, Kyoto 606, Japan

Received 22 May 1989

Abstract. An $S = \frac{3}{2}$ Heisenberg antiferromagnet on a triangular lattice $CuCrO_2$, in which stacking of the triangular lattice of magnetic Cr atoms forms a layered rhombohedral antiferromagnet, is studied by neutron powder diffraction. In the paramagnetic phase the powder diffraction pattern shows asymmetry, which proves a two-dimensional character. In the ordered phase, magnetic Bragg scattering has large width, indicating that the scattering is distributed on a line $(\frac{1}{3}\frac{1}{3}\zeta)$ with peaks where ζ takes integer values. Although the magnetic long-range order is established in the c plane, correlation in the c direction is finite or the modulation vector is distributed on the line. Intensity of magnetic reflections is consistent with the 120° structure in the a–c plane with moment $(3.1 \pm 0.2)\mu_B$.

1. Introduction

Heisenberg antiferromagnets on a triangular lattice (HAFT) have been shown to have interesting magnetic properties [1–3]. For a classical spin ($S = \infty$) HAFT, Kawamura and Miyashita (KM) [1] found an intriguing phase transition at a finite temperature T_{KM} whereas $T_c = 0$ in a Heisenberg ferromagnet in two dimensions. In a non-collinear spin configuration of the ground-state 120° structure, a topological excitation named the Z_2 vortex can stably exist; thus the phase transition at $T_{KM} > 0$ which is characterised by dissociation of the Z_2 vortex takes place. Experimental studies of a quasi-two-dimensional HAFT have been performed on VX_2 ($X \equiv Cl$, Br) [4] and AMO_2 ($A \equiv Li$, Na, K and $M \equiv Ti$, Cr, Ni) [5–9]; however, purely two-dimensional nature has not been well studied. Materials which show highly two-dimensional behaviour and are suitable for the KM transition have been sought. In this study we performed neutron scattering experiments on a polycrystalline AMO_2 family compound, $CuCrO_2$, on which Ajiro *et al* [9] measured the ESR linewidth to investigate the activation of the Z_2 vortex. We have proved a quasi-two-dimensional behaviour in the paramagnetic phase and determined a magnetic structure in the antiferromagnetically ordered phase.

§ Present address: Government Industrial Research Institute, Nagoya, Kita-ku, Nagoya 462, Japan.

0953-8984/90/194485 + 09 $03.50

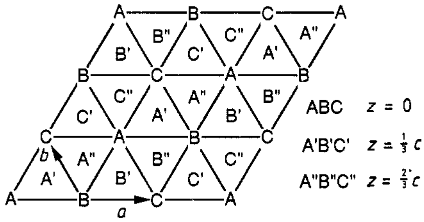

Figure 1. Crystal structure of Cr atoms. Nine sublattices of magnetic structure are represented by ABC, A′B′C′ and A″B″C″ in $z = 0, \frac{1}{3}c, \frac{2}{3}c$ planes, respectively.

The compound $CuCrO_2$ crystallises in the delafossite ($CuFeO_2$) structure [10] which belongs to the space group R$\bar{3}$m. It consists of layers of triangular lattices in a sequence O^{2-}–Cr^{3+}–O^{2-}–Cu^{+}–O^{2-}–Cr^{3+}–. Since the $(3d)^3$ electronic state of the magnetic ion Cr^{3+} surrounded by an octahedron of O^{2-} has a quenched orbital moment, its magnetic properties are well represented by $S = \frac{3}{2}$ Heisenberg spins. The stacking sequence of the Cr^{3+} triangular lattices is ABCABC . . . type as illustrated in figure 1; that is, $CuCrO_2$ is a quasi-two-dimensional antiferromagnet on a rhombohedral lattice. The Hamiltonian can be written as

$$H = 2J \sum_{\langle ij \rangle} \boldsymbol{S}_i \cdot \boldsymbol{S}_j + 2J' \sum_{\langle l,m \rangle} \boldsymbol{S}_l \cdot \boldsymbol{S}_m + D \sum_i (S_i^z)^2 \tag{1}$$

where the first and the second terms are the nearest-neighbour exchange coupling in and between the layers and D is a small anisotropy constant. From the crystal structure $|J'| \ll J$ is expected. In fact, susceptibility measurements by Doumerc *et al* [8] showed that it has a Néel temperature T_N of 27 K and that the susceptibility at high temperatures is well accounted for by a high-temperature expansion using the first intra-layer term of equation (1) with $J/k_B = 11.4$.

If the inter-layer coupling and the anisotropy could be neglected, the transition temperature would be $T_{KM} = 0.31(2J)S^2 = 15.9$ K [1]. Since this value is 40% smaller than the observed Néel temperature, the phase transition is largely affected by the inter-layer coupling or the anisotropy. The anisotropy of $CuCrO_2$ will be shown to be the easy-axis type in a later section. The influence of an easy-axis anisotropy on the phase transition was studied by Miyashita [2]. He showed that the anisotropy separates T_{KM} into two phase transitions with uniaxial and in-plane symmetries, a phase diagram of which is shown in figure 8 of [2]. Judging from this phase diagram and no apparent double-phase transition in $CuCrO_2$, we think that not the anisotropy but the inter-layer coupling is responsible for the fact that T_N is increased from T_{KM}.

From the viewpoint of a three-dimensional system, $CuCrO_2$ is a rhombohedral antiferromagnet which may undergo a peculiar phase transition. Rastelli and Tassi [11] pointed out that the ground-state spin configuration of a rhombohedral antiferromagnet is highly degenerate helical ordering. Its modulation vector $\boldsymbol{Q}$ has infinite degeneracy on a line in the reciprocal space; that is, $J(\boldsymbol{Q})$ takes a minimum on the line. For small $|J'/J|$ the line is approximately given by

$$\begin{aligned} \boldsymbol{Q} &= \tfrac{1}{3}(\boldsymbol{a}^* + \boldsymbol{b}^*)(1+u) + (1/\sqrt{3})(\boldsymbol{b}^* - \boldsymbol{a}^*)v + \boldsymbol{c}^* w \\ u &= (\sqrt{3}/2\pi)(J'/J)\cos(2\pi w/3) \\ v &= -(\sqrt{3}/2\pi)(J'/J)\sin(2\pi w/3) \end{aligned} \tag{2}$$

where u and v are orthogonal coordinates in the c plane. The projection of the line to

Table 1. Observed and calculated structure factors of $CuCrO_2$ at $T = 9$ K (space group, $R\bar{3}m$; atomic positions, Cu (0, 0, 0), Cr(0, 0, $\frac{1}{2}$) and O (0, 0, z), $z = 0.1078(3)$).

(h, k, l)	$\lvert F_{obs} \rvert$	$\lvert F_{calc} \rvert$
(0, 0, 3)	0.32	0.30
(0, 0, 6)	1.32	1.27
(1, 0, 1)	3.93	3.96
(0, 1, 2)	4.13	4.11
(0, 1, 5)	2.27	2.13
(0, 0, 9)	4.49	4.67
(1, 0, 7)	1.25	1.35

the c plane is a circle with centre at $(\frac{1}{3}\frac{1}{3}0)$, which is a Bragg point of the 120° structure. Owing to this degeneracy, the long-range order of this helical structure is unstable at finite temperatures for purely Heisenberg spin [11]. A zero-temperature critical point or a power-law decay phase might be expected. In $CuCrO_2$ a smaller perturbation, for instance second- or third-neighbour inter-layer exchange, brings about the three-dimensional ordering. It should be noted that, in spite of appreciable J', the degeneracy line may give rise to effectively two-dimensional behaviour in the paramagnetic phase, which we shall show by the asymmetry of the powder pattern in a later section.

2. Experimental details and results

A powder specimen of $CuCrO_2$ was prepared by solid state reaction from a stoichiometric mixture of CuO and Cr_2O_3, which was heated in air at 1050 °C for 48 h [8]. The neutron scattering experiments were performed on the ISSP-ND-I triple-axis spectrometer installed at JRR-2 JAERI (Tokai) with the double-axis configuration. A pyrolytic graphite (002) reflection was used for the monochromator. Higher-order neutrons were removed by the pyrolytic graphite filter. The neutron energy was fixed at 13.7 meV, and the collimation 80′–30′–20′ was employed. The sample was mounted in a closed-cycle He refrigerator.

Integrated intensities of the nuclear reflections were measured up to $2\theta = 90°$ at $T = 9$ K. Because of the limited number of the reflections, we performed a structure refinement with one fitting parameter of the oxygen position, $(00z)$, where temperature factors and atomic occupations are fixed to $B = 0$ and 100%, respectively. The results are summarised in table 1. The observed structure factors agree well with the calculation.

Powder diffraction patterns have been measured at several temperatures. The data taken at the lowest temperature $T = 9$ K are shown in figure 2. One can see from this figure that magnetic reflections indexed by $(\frac{1}{3}\frac{1}{3}l)$ and $(\frac{2}{3}\frac{2}{3}l)$, $l = 0, 1, 2, \ldots$, appear. The width of the $(\frac{1}{3}\frac{1}{3}l)$ series, which is smallest for $l = 0$ and increases as l becomes larger, is wider than the instrumental resolution which gives narrower nuclear Bragg peaks. Furthermore the magnetic reflections overlap each other. These mean that the Bragg points are distributed on a line $(\frac{1}{3}\frac{1}{3}\zeta)$ with peaks where ζ takes integer values. It should be noted that the same phenomenon was observed in the previous powder neutron measurement on $NaCrO_2$ [6], which has the same lattice of the magnetic ions. We think that these ill defined Bragg peaks have a close relation to the degeneracy line in the

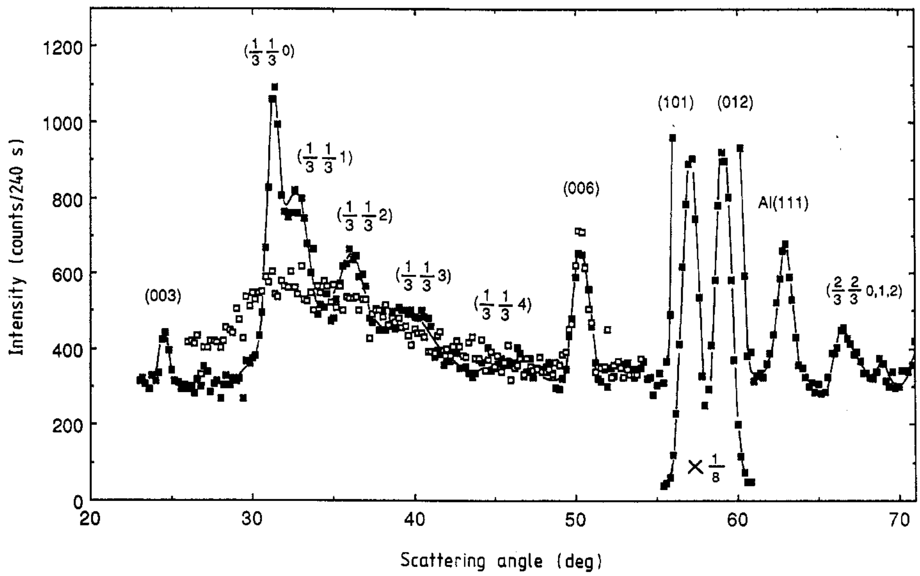

Figure 2. Neutron diffraction pattern for $CuCrO_2$ at $T = 9$ K ($< T_N$) (■) and $T = 32$ K ($> T_N$) (□).

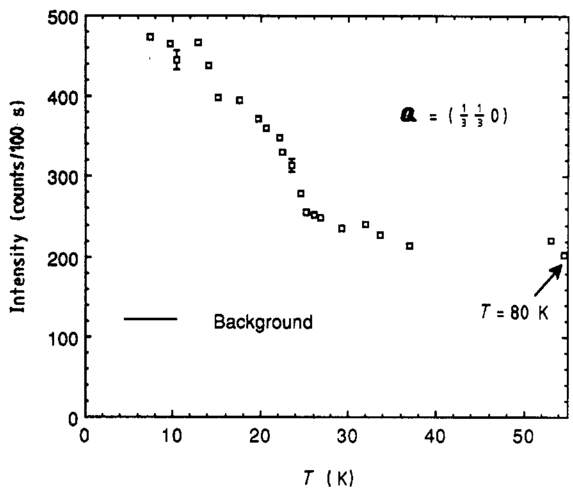

Figure 3. Temperature dependence of the $(\frac{1}{3}\frac{1}{3}0)$ peak intensity for $CuCrO_2$.

rhombohedral antiferromagnet explained in the previous section. In the quasi-two-dimensional case the line, equation (2), can be well approximated by $(\frac{1}{3}\frac{1}{3}\zeta)$. Therefore, if the modulation wavevector in each small crystal varies on the line, smearing of the Bragg points can occur. Alternatively, the smearing indicates that long-range order is established only in the c plane, but the spin-correlation length is finite in the c direction. This can be brought about by a perturbation of crystal imperfections such as deficiencies, magnetic moments of Cu^{2+}, and holes at the oxygen site.

The temperature dependence of the $(\frac{1}{3}\frac{1}{3}0)$ peak intensity has been measured and is shown in figure 3. The Néel temperature is $T_N = 25 \pm 0.5$ K, which is consistent with the previous susceptibility measurement [8]. As seen from this figure, the large intensity relative to the background remains far above T_N up to at least 80 K. The magnetic diffraction pattern above T_N is plotted also in figure 2. High asymmetry, which is evident in the shape, shows that two-dimensional short-range order has a long correlation over a very wide temperature range, which is also in accord with the degeneracy line in the rhombohedral antiferromagnet.

Because of the spread of the magnetic Bragg points in the c direction, determination of the magnetic structure has certain ambiguity. We shall discuss an averaged spin structure in the following way. We assume that in a perfect crystal the Bragg line $(\frac{1}{3}\frac{1}{3}\zeta)$ would be Bragg points $(\frac{1}{3}\frac{1}{3}l)$, and that their integrated intensities can be estimated from an appropriate fit in which the observed diffraction pattern of $(\frac{1}{3}\frac{1}{3}\zeta)$ is fitted to five Gaussian peaks. The resulting magnetic intensities are listed in table 2, where they are further reduced to structure factors using the calculated form factor [12] and an approximate g-factor of 2 [9]. Here the magnetic structure factor is defined as

$$|F_M|^2 = |\boldsymbol{F}_M|^2 - |(\hat{\boldsymbol{Q}} \cdot \boldsymbol{F}_M)|^2$$

$$\boldsymbol{F}_M = \sum_{\text{unit cell}} \boldsymbol{S}_r \exp(\mathrm{i}\boldsymbol{Q} \cdot \boldsymbol{r}).$$

The index of the magnetic reflection means that the magnetic unit cell contains three Cr^{3+} sites in the c plane and three Cr^{3+} layers in the c direction. The nine sublattice Cr^{3+} sites in the magnetic unit cell are illustrated in figure 1 by ABC, A′B′C′ and A″B″C″. Since the limited number of the reflections prohibits us from determining the configuration of the nine spins, we furthermore assume that all spins are in one plane, and that the three sublattice spins in each layer have zero total spin:

$$\boldsymbol{S}_A + \boldsymbol{S}_B + \boldsymbol{S}_C = \boldsymbol{0}, \ldots.$$

We have tried to calculate intensities of a number of spin structures. Several typical structures giving a relatively good fit are depicted in figure 4. The spins at the nine sites in figure 1 are represented by arrows, half-arrows and full circles (zero moment). For example, in the structure in figure 4(a), the three sublattice spins in a layer make an angle of 120° between each other and the nine spins are in the same plane including the c axis. The spins at the sites A, A′, and A″ tilt from the c axis by angles 0, $\theta_{A'}$, and $\theta_{A''}$, respectively.

For the 120° structures (figures 4(a)–4(d)), since good agreement is obtained in very large regions in $(\theta_{A'}, \theta_{A''})$ space, we show contour maps of the χ^2-values in figure 5, where χ^2 is defined by

$$\chi^2 = \sum \left(\frac{|F_{\text{obs}}|^2 - |F_{\text{calc}}|^2}{\sigma(|F_{\text{obs}}|^2)} \right)^2$$

which is minimised by adjusting the spin moment. It should be noted that the moment depends weakly on $\theta_{A'}$ and $\theta_{A''}$. Since there are six observed intensities and three adjustable parameters (the spin moment, $\theta_{A'}$ and $\theta_{A''}$), χ^2 is distributed in a χ^2 distribution with three degrees of freedom. Applying the χ^2 test at a 5% level of significance, the models which give $\chi^2 < 8$ are accepted. Contours of $\chi^2 = 8$ are plotted as broken curves in figure 5, which enclose very wide ranges. The calculated structure factors, the χ^2-values and the moments of the four typical spin configurations in figures 4(a)–4(d) are listed in table 2, which shows good agreement with the observations. We also performed the same procedure for the 120° structures where the spins are in the c plane. However,

Table 2. Observed and calculated squares of magnetic structure factors of $CuCrO_2$ at $T = 9$ K. The averaged value is used for $(\frac{2}{3}\frac{2}{3}l)$, $l = 0, 1, 2$. The structures in figure 4 are models of the calculations. In the last two rows, the spin moment μ (gS_A for figures 4(*a*)–(*e*) and gS_B for figure 4(*f*)) and the χ^2 are listed.

		$\lvert F_{calc}\rvert^2$					
(h, k, l)	$\lvert F_{obs}\rvert^2$	Figure 4(*a*) $\theta_{A'} = 0$ $\theta_{A''} = 0$	Figure 4(*b*) $\theta_{A'} = 0$ $\theta_{A''} = -165°$	Figure 4(*c*) $\theta_{A'} = -165°$ $\theta_{A''} = 0$	Figure 4(*d*) $\theta_{A'} = -160°$ $\theta_{A''} = -160°$	Figure 4(*e*)	Figure 4(*f*)
$(\frac{1}{3}\frac{1}{3}0)$	19.2	20.3	20.8	20.8	20.8	15.0	15.0
$(\frac{1}{3}\frac{1}{3}1)$	13.3	12.5	12.2	12.2	12.1	14.7	14.7
$(\frac{1}{3}\frac{1}{3}2)$	15.0	12.1	13.8	13.8	14.4	13.9	13.9
$(\frac{1}{3}\frac{1}{3}3)$	15.6	16.4	16.8	16.8	16.9	13.1	13.1
$(\frac{1}{3}\frac{1}{3}4)$	10.4	11.4	10.2	10.2	9.7	12.4	12.4
$(\frac{2}{3}\frac{2}{3}0, 1, 2)$	14.4 (average)	14.1	14.4	14.4	14.5	14.8	14.8
μ/μ_B		3.0 ± 0.1	3.1 ± 0.1	3.1 ± 0.1	3.1 ± 0.1	5.9 ± 0.2	5.1 ± 0.2
χ^2		5.6	2.7	2.7	2.9	13.5	13.5

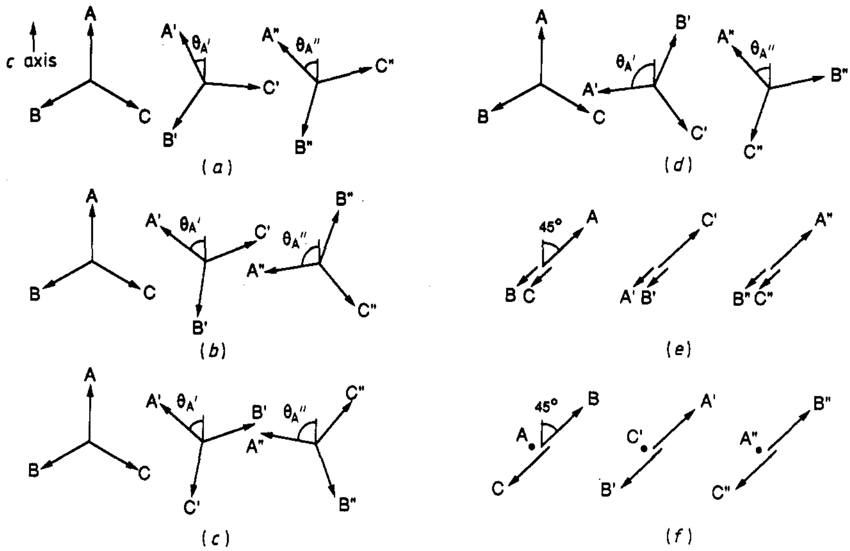

Figure 4. Magnetic structure models. The arrows and dots (zero vector) represent spins at the nine sublattices shown in figure 1.

the χ^2-values are always larger than 57, which means that the fits are far worse and unacceptable. Therefore we conclude that the 120° structures in the *a–c* plane with moment $(3.1 \pm 0.2)\mu_B$ can reproduce the magnetic intensities; however, the mutual spin angles and the rotation sense of the layers cannot be obtained from the data. The magnitude of the moment is consistent with $S = \frac{3}{2}$ and $g \approx 2$.

We also tried numerous collinear spin structures in which the three sublattice spins in the layer have different moments and satisfy the constraint of zero total spin. The best fit is obtained for several structures, simplest examples of which are shown in figures 4(*e*) and 4(*f*). The lowest χ^2-value is 13.5. The calculated structure factors of these structures are summarised in table 2, in which one can see that the agreement is not as satisfactory as the 120° structures, because the calculation of $(\frac{1}{3}\frac{1}{3}0)$ is somewhat smaller than the observations. In fact, if we apply the χ^2 test, the models are rejected at a 1% level of significance. Therefore we conclude that the collinear spin structures are not capable of reproducing the intensities.

3. Conclusions

We have carried out neutron powder diffraction measurements on polycrystalline $CuCrO_2$. Over the wide temperature range in the paramagnetic phase, the diffraction pattern shows asymmetry which proves the two-dimensional character. Below T_N the antiferromagnetic diffraction pattern is very broad, which indicates that two-dimensional long-range order is established in the *c* plane, whereas correlation in the *c* direction is finite, or that the modulation vector is distributed on the line $(\frac{1}{3}\frac{1}{3}\zeta)$. Assuming that the diffraction pattern is concentrated on the Bragg positions $(\frac{1}{3}\frac{1}{3}l)$ where l is an integer, we analysed the averaged spin structure under the two following restrictions: the nine sublattice spins are in one plane; the three sublattice spins in the layer have zero total

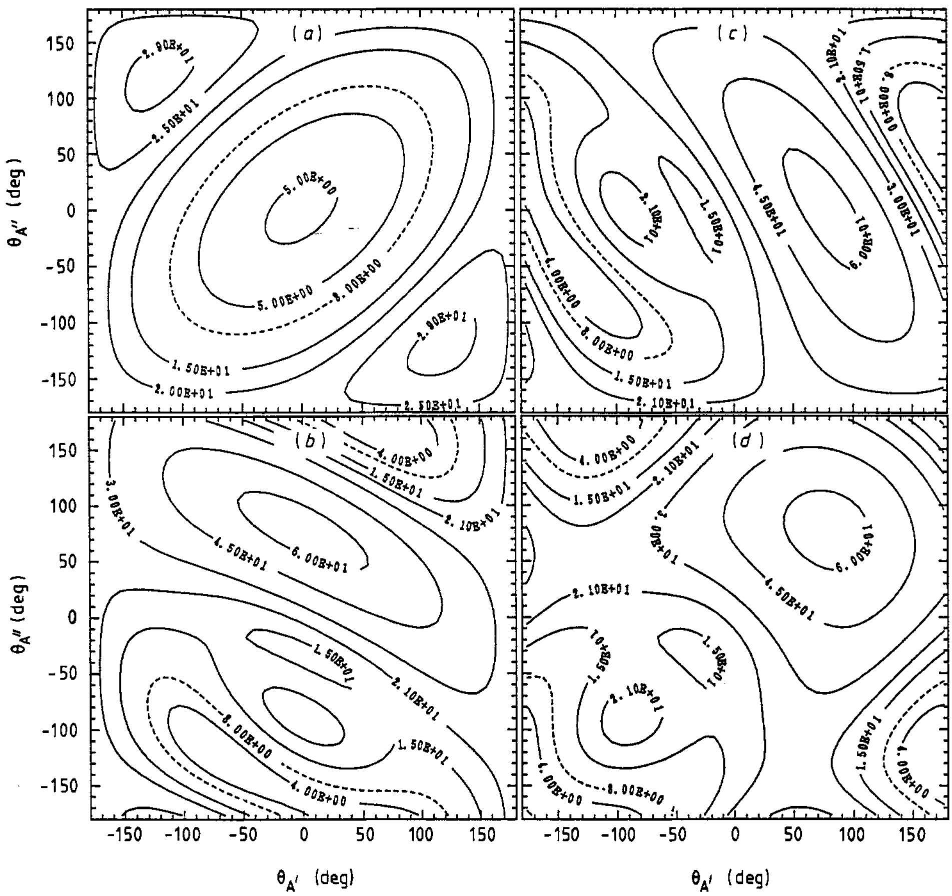

Figure 5. Contour map of χ^2 defined in the text in $(\theta_{A'}, \theta_{A''})$ space: - - -, contours of $\chi^2 = 8$. (*a*), (*b*), (*c*) and (*d*) correspond to the structure models shown in figures 4(*a*), 4(*b*), 4(*c*) and 4(*d*) respectively.

spin. The intensities of the magnetic reflections are reproduced by the 120° structure in the *a*–*c* plane with moment $(3.1 \pm 0.2)\mu_B$, which is illustrated in figures 4(*a*)–4(*d*), where the mutual angles and the sense of the rotation between the spins in the three sublattice layers are very ambiguous. This structure shows that the model Hamiltonian (equation (1)) has easy-axis anisotropy, $D < 0$.

Acknowledgments

We would like to thank Dr H Yoshizawa for valuable discussions and Dr S Sato for explanation of the use of a structure refinement program.

References

[1] Kawamura H and Miyashita S 1984 *J. Phys. Soc. Japan* **53** 9, 4138

[2] Miyashita S and Kawamura H 1985 *J. Phys. Soc. Japan* **54** 3385
[3] Andeson P W 1973 *Mater. Res. Bull.* **8** 153
Fazekas P and Anderson P W 1974 *Phil. Mag.* **30** 423
[4] Niel M, Cros C, Le Flem G, Pouchard M and Hagenmuller P 1977 *Physica* B + C **86–8** 702
Hirakawa K, Kadowaki H and Ubukoshi K 1983 *J. Phys. Soc. Japan* **52** 1814
Kadowaki H, Ubukoshi K and Hirakawa K 1985 *J. Phys. Soc. Japan* **54** 363
Yamada I, Ubukoshi K and Hirakawa K 1984 *J. Phys. Soc. Japan* **53** 381
Takeda K, Ubukoshi K, Haseda T and Hirakawa K 1984 *J. Phys. Soc. Japan* **53** 1480
Kadowaki H, Ubukoshi K and Hirakawa K 1987 *J. Phys. Soc. Japan* **56** 4027
[5] Hirakawa K, Kadowaki H and Ubukoshi K 1985 *J. Phys. Soc. Japan* **54** 3526
Yamada I, Ubukoshi K and Hirakawa K 1985 *J. Phys. Soc. Japan* **54** 3571
[6] Soubeyroux J L, Fruchart D, Delmas C and Le Flem G 1979 *J. Magn. Magn. Mater.* **14** 159
[7] Soubeyroux J L, Fruchart D, Marmeggi J C, Fitzgerald W J, Delmas C and Le Flem G 1981 *Phys. Status Solidi* **67** 633
[8] Doumerc J-P, Wichainchai A, Ammar A, Pouchard M and Hagenmuller P 1986 *Mater. Res. Bull.* **21** 745
[9] Ajiro Y, Kikuchi H, Sugiyama S, Nakashima T, Shamoto S, Nakayama N, Kiyama M, Yamamoto N and Oka Y 1988 *J. Phys. Soc. Japan* **57** 2268
Ajiro Y *et al* to be published
[10] Prewitt C T, Shannon R D and Rogers D B 1971 *Inorg. Chem.* **10** 719
[11] Rastelli E and Tassi A 1986 *J. Phys. C: Solid State Phys.* **19** L423; 1988 *J. Phys. C: Solid State Phys.* **21** 1003
[12] Watson R E and Freeman A J 1961 *Acta Crystallogr.* **14** 27